Regge-Pole Model for the Secondary Maxima in πN and NN Scattering and the No-Compensation Mechanism*

CHARLES B. CHIU, SHU-YUAN CHU, AND LING-LIE WANG
Lawrence Radiation Laboratory, University of California, Berkeley, California
(Received 1 February 1967, revised manuscript received 29 May 1967)

The dip-bump structure in the low-energy $\pi^{\pm}p$ elastic differential cross section has been studied. We find that a zero in the helicity nonflip amplitude of the P' trajectory gives a natural explanation of this structure. At the same time we have consistently fitted the high-energy $\pi^{\pm}p$ total and differential cross sections, the $\pi^{\pm}p$ polarizations, and the π^-p charge-exchange differential cross-section data. The helicity nonflip amplitude of the P' trajectory will vanish at $\alpha_{P'}=0$ if the P' trajectory chooses what we call the no-compensation mechanism. Consistent with our $\pi^{\pm}p$ solution, the pp and $\bar{p}p$ total and differential cross sections can also be well fitted. The secondary maximum in the low-energy $\bar{p}p$ differential cross section is reproduced.

I. INTRODUCTION

THE secondary bumps in $\pi^{\pm}p$ elastic scattering have been measured extensively by Coffin *et al.* of the Michigan Group.[1,2] Some of the data are shown in Fig. 1.[3] One sees that the general feature and the magnitude of the dip and the secondary bump for both π^+p and π^-p are roughly the same. They are quite pronounced at 2.5 GeV/c and decrease rapidly with the increase of energy. The similarity between π^+p and π^-p secondary bumps and their smooth energy dependence imply that these bumps cannot be dominated by the direct channel resonances, instead they are dominated by the t-channel ($\pi\pi \to N\bar{N}$) exchange contributions. The contribution to the differential cross section (DCS) due to the t-channel exchange of an isospin 0 state is given by the expression

$$\frac{d\sigma}{dt}(I=0)=\frac{1}{2}\left[\frac{d\sigma}{dt}(\pi^+p\to\pi^+p)+\frac{d\sigma}{dt}(\pi^-p\to\pi^-p)-\frac{d\sigma}{dt}(\pi^-p\to\pi^0n)\right]. \quad (1.1)$$

Since the charge-exchange secondary bump at the same energy is about a factor of four smaller than the bumps in the elastic DCS,[4] the resultant $(d\sigma/dt)(I=0)$ should be very similar to that shown in Fig. 1. We have checked that $(d\sigma/dt)(I=0)$ in the secondary bump region can be approximately fitted in a model-independent way by the formula

$$\frac{d\sigma}{dt}=F(t)E_L^{2\alpha_{\rm eff}(t)-2}. \quad (1.2)$$

The value of $\alpha_{\rm eff}(t)$ is quite negative. For instance, at $t=-1.4$ (GeV/c)^2, near the peak of the secondary bump, $\alpha(t)$ for the rapid fall below 8 GeV/c is somewhere between -0.4 and -0.9. Recently dips in the DCS have been associated with the vanishing of Regge trajectories;[5-7] thus it is natural to attempt to explain these dip-bump structures by the Regge-pole mode. In this paper, as usual, we assume the $I=0$ state t-channel exchange is dominated by the Regge trajectories P and P'. We assume the P trajectory is relatively flat, as is suggested by the observed nonshrinking diffraction peak near the forward direction at high energy and by the earlier fits to the high-energy pion-nucleon data.[8] Then the low value of $\alpha(t)$ in the secondary-bump region implies that the secondary bump has to be associated with the P' trajectory rather than the P trajectory. The zero intercept of P' has been determined by various authors[9] to be above 0.5, so the P' trajectory has to be relatively steep. It has been suggested by Frautschi[10] that, as in the $\pi^-p\to\pi^0n$ case, the vanishing of the helicity-flip amplitude[11] of P', $f_{sn}{}^{P'}$, at $\alpha_{P'}=0$ could be used to explain the secondary bump in the elastic DCS.[12] We investigated this possibility (Chew mechanism) extensively by fitting the secondary bump shown in Fig. 1, together with the high-energy data.[8] Our solutions, with reasonable fits to the secondary bump, do not have good χ^2 values for the high-energy data. However, a different possibility

* Work done under auspices of the U. S. Atomic Energy Commission.

[1] C. T. Coffin, N. Dikmen, L. Ettlinger, D. Meyer, A. Saulys, K. Terwilliger, and D. Williams, Phys. Rev. Letters **15**, 838 (1965).

[2] C. T. Coffin, N. Dikmen, L. Ettlinger, D. Meyer, A. Saulys, K. Terwilliger, and D. Williams, Phys. Rev. Letters **17**, 458 (1966).

[3] Data in Fig. 1 also included the work of K. J. Foley, S. J. Lindenbaum, W. A. Love, S. Ozaki, J. J. Russell, and L. C. L. Yuan, Phys. Rev. Letters **11**, 425 (1963); J. Orear, R. Rubinstein, D. B. Scarl, D. H. White, A. D. Krisch, W. R. Frisken, A. L. Read, and H. Ruderman, Phys. Rev. **152**, 1162 (1966).

[4] For charge-exchange DCS data see A. S. Carroll, I. F. Corbet, C. J. S. Damerell, N. Middlemas, D. Newton, A. B. Clegg, and W. S. C. Williams, Phys. Rev. Letters **16**, 288 (1966); P. Sonderegger, J. Kirz, O. Guisan, P. Falk-Vairant, C. Bruneton, P. Borgeaud, A. V. Stirling, C. Caverzasio, J. Guillaud, M. Yvert, and B. Amblard, Phys. Letters **20**, 75 (1966).

[5] G. Höhler, J. Baacke, H. Schlaile, and P. Sonderegger, Phys. Letters **20**, 79 (1966); F. Arbab and C. Chiu, Phys. Rev. **147**, 1045 (1966).

[6] C. Chiu and J. Stack, Phys. Rev. **153**, 1575 (1967).

[7] L. L. Wang, Phys. Rev. Letters **16**, 756 (1966).

[8] The high-energy data we used are essentially the same as those used by C. Chiu, R. J. N. Phillips, and W. Rarita, Phys. Rev. **153**, 1485 (1967).

[9] J. Scanio, Phys. Rev. **152**, 1337 (1966); M. Restignoli, L. Sertorio, and M. Toller, *ibid* **150**, 1389 (1966).

[10] S. Frautschi, Phys. Rev. Letters **17**, 722 (1966).

[11] See Sec. II for the detailed definition of helicity amplitudes.

[12] See also solution b of Ref. 8.

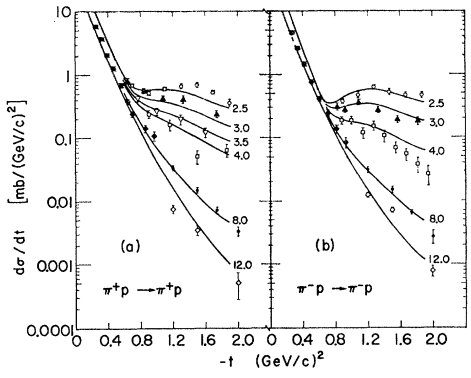

FIG. 1. The $\pi^{\pm}p$ differential cross sections π^+p—○, 2.5 GeV/c; ▲, 3; ▽, 3.5; □, 4 GeV/c by Coffin *et al.*, from Ref. 2; (black diamond) at 6.8 GeV/c by Foley *et al.*, from Ref. 3; ● at 8 and ◇ at 12 GeV/c by Orear *et al.*, from Ref. 3. π^-p—○, 2.5 GeV/c, ▲, 3 GeV/c, and □, 4 GeV/c by Coffin *et al.* from Ref. 1; (black diamond) at 7 GeV/c by Foley *et al.* from Ref. 3; ● and ◇ at 8 and 12 GeV/c by Orear *et al.*, from Ref. 3. The solid curves are our fits with no-compensation mechanism.

is that the helicity-nonflip amplitude of P' can vanish at $\alpha_{P'}=0$, if the P' trajectory chooses what we call the "no-compensation mechanism."[13,14] The no-compensation mechanism for P' means that P' couples to the nonsense channel, and *the residue of the nonsense-nonsense amplitude vanishes*. Thus there is no pole in the nonsense-nonsense amplitude, and it is not necessary to have a compensating trajectory to cancel the pole, as needed for the Gell-Mann mechanism. This possibility offers a new way to explain the observed secondary bumps, and we found that the dip-bump structure, indeed, can be explained naturally by the vanishing of the nonhelicity-flip amplitude, $f_{ss}{}^{P'}$, at $\alpha_{P'}=0$; namely, by introducing an extra factor of $\alpha_{P'}$ to the amplitude $f_{ss}{}^{P'}$.

In Sec. II we discuss in some detail the four possible ways of assigning the α factors to the various helicity amplitudes of pion-nucleon and nucleon-nucleon scattering. This will serve as the basis of our parametrization. In Sec. III, we discuss our fits to the pion-nucleon data. In Sec. IV we present our analysis on the nucleon-nucleon data, where we show that, consistent with our πN solution, both the observed smooth pp DSC and the structured $\bar{p}p$ DCS can also be adequately fitted.

II. FOUR DIFFERENT WAYS OF ASSIGNING THE α FACTORS

When the total angular momentum α of a system is less than its total intrinsic spin polarization, its value becomes unphysical. A system at such an unphysical integral value of α has been called a "nonsense state." For example, at $\alpha=0$, any state with nonzero total helicity is a nonsense state. To be specific, we discuss[15] a system with total helicity 0 or 1. The generalization to states with other values of total helicity is straightforward. The s-channel differential cross section, expressed in terms of t-channel helicity amplitudes, is given by

$$\frac{d\sigma}{dt}=\frac{1}{4\pi s p^2}[|f_{ss}|^2+a|\sin\theta_t|^2|f_{sn}|^2 +b[1+(\cos\theta_t)^2]|f_{nn}|^2], \quad (2.1)$$

where the subscript s stands for sense and n stands for nonsense with respect to $\alpha=0$; p is the initial momentum in the s-channel center-of-mass system; the f's are the t-channel helicity amplitudes suitable for Reggeization; $a=1$, $b=0$ for $\pi N\to\pi N$ and $a=2$, $b=1$ for $NN\to NN$ or $N\bar{N}\to N\bar{N}$. The leading terms with the highest power in s, in terms of the t-channel Regge-pole parameters, are[16]

$$f_{ss}\sim\eta(t)\beta_{ss}(t)\left(\frac{s}{qq'}\right)^{\alpha(t)}, \quad (2.2a)$$

$$f_{sn}\sim\eta(t)\beta_{sn}(t)\frac{2\alpha}{[\alpha(\alpha+1)]^{1/2}}\left(\frac{s}{qq'}\right)^{\alpha-1}, \quad (2.2b)$$

$$f_{nn}\sim\eta(t)\beta_{nn}(t)\frac{2\alpha}{\alpha+1}\left(\frac{s}{qq'}\right)^{\alpha-1}, \quad (2.2c)$$

where

$$\eta(t)\equiv\frac{-[\exp(-i\pi\alpha)\pm1]}{\sin\pi\alpha}\times\frac{(2\alpha+1)\Gamma(\alpha+\frac{1}{2})}{\pi^{1/2}\Gamma(\alpha+1)},$$

The β's are the unmodified residue functions of the Regge pole, and q, q' are the initial and the final momenta in the t-channel center-of-mass system, respectively. So far all the α factors come from the asymptotic form of the generalized Legendre functions for large s. The β's are factorizable, i.e.,

$$[\beta_{sn}(t)]^2=\beta_{ss}(t)\beta_{nn}(t). \quad (2.3)$$

At $\alpha=0$ and its symmetric point about $\alpha=-\frac{1}{2}$, namely, $\alpha=-1$,

$$\beta_{sn}(t)\propto\{\alpha(t)[\alpha(t)+1]\}^{1/2}. \quad (2.4)$$

Physically Eq. (2.4) says that the sense state and the nonsense state decouple at $\alpha=0$ and $\alpha=-1$.[17] Except

[13] We have studied the $N\bar{N}$ system in the potential theory of this no-compensation mechanism. We find that the residues do not vanish at $\alpha=0$, and thus the no-compensation mechanism cannot occur here. This is because $\alpha=0$ is the first nonsense value in the $N\bar{N}$ system. However, from this study it is very plausible that this mechanism can occur in higher spin systems, where $\alpha=0$ will be the second or third nonsense value. We thank Professor S. Mandelstam and Chung-I Tan for helpful discussions on this study.

[14] L. L. Wang, Phys. Rev. **153**, 1664 (1967). This particular mechanism, which gives a zero at $\alpha_{P'}=0$ in the helicity-nonflip amplitude, and the Chew mechanism are mentioned in Footnote 14 of this reference.

[15] The possibilities of assigning the α factors have been briefly discussed in the Footnotes 9, 10, and 14 of Ref. 14. For completeness we discuss these factors in detail here.

[16] We assume that the fixed pole contribution in the J plane is not important. For details in the fixed pole contribution see S. Mandelstam and L. Wang, Phys. Rev. **160**, 1490 (1967).

[17] M. Gell-Mann, M. Goldberger, F. Low, and F. Zachariasen, Phys. Rev. **133**, B145 (1964).

for the known threshold and some t-kinematic factors,[18] the β's are analytic in t for $t<0$. Therefore, from Eq. (2.3), the α factors of β_{sn} must appear in either β_{ss} or β_{nn}. It can happen in four different ways depending upon the dynamics of the system:

(1) *Choosing-sense mechanism.* The trajectory couples to the ss (sense-sense) amplitude, so the residue of nn (nonsense-nonsense) amplitude vanishes, i.e., $\beta_{ss}\propto 1$, $\beta_{sn}\propto[\alpha(\alpha+1)]^{1/2}$, $\beta_{nn}\propto\alpha(\alpha+1)$.

(2) *Chew's mechanism.*[19] The trajectory does couple to the ss amplitude, but for some dynamical reason the residue function of the ss amplitude vanishes at $\alpha=0$. To satisfy both Eqs. (2.3) and (2.4), one finds

$$\beta_{ss}\propto\alpha,\quad \beta_{sn}\propto\alpha[\alpha(\alpha+1)]^{1/2},\quad \beta_{nn}\propto\alpha^2(\alpha+1).$$

(3) *Gell-Mann's mechanism.*[20] The trajectory couples to the nonsense channel, and the pole in the nn amplitude is canceled by a compensating trajectory with opposite parity passing $\alpha=-1$. Therefore there is no pole in the full helicity amplitude at $\alpha=0$. In this case,

$$\beta_{ss}\propto\alpha(\alpha+1),\quad \beta_{sn}\propto[\alpha(\alpha+1)]^{1/2},\quad \beta_{nn}\propto 1.$$

The contribution from the compensating trajectory with opposite parity is not written out in Eqs. (2.2), because it has lower power in s away from $\alpha=0$.

(4) *No-compensation mechanism.* The trajectory does couple to the nonsense channel, but the residue of the nn amplitude vanishes at $\alpha=0$; thus the compensating trajectory is not necessary. We have

$$\beta_{ss}\propto\alpha^2(\alpha+1),\quad \beta_{sn}\propto\alpha\{\alpha(\alpha+1)\}^{1/2},\quad \beta_{nn}\propto\alpha.$$

Until we know the dynamics, we cannot decide theoretically which mechanism is the correct one for a given trajectory. However, by fitting the data, we can find out which mechanism is consistent with the experimental situation.

In the case of the ρ trajectory, one studies the reaction $\pi^-p\to\pi^0n$. Here the choosing-sense mechanism has been used by various authors to explain the data consistently.[5] In the absence of explicit parametrization of the background contribution,[21] their choice is favored for the following reasons. The cross section near the dip is sizable, so it is natural to choose the mechanism where $f_{ss}{}^{\rho}$ does not vanish at $\alpha_\rho=0$. Secondly, this choice is also consistent with the observed small and yet statistically significant positive difference[22] between the π^+p and π^-p DCS at high energy in the t region between -0.4 and -0.8 $(\mathrm{GeV}/c)^2$. Otherwise if both $f_{ss}{}^{\rho}$ and $f_{sn}{}^{\rho}$ vanish at $\alpha_\rho=0$, one would expect the difference to change sign in this t interval. In spite of these arguments, we feel that a detailed study of the energy dependence of the magnitude of the dip and more accurate measurement of the difference in π^+p and π^-p DCS eventually will be needed to make this choice conclusive.

For the ω trajectory one studies the difference between pp and $\bar{p}p$ elastic DCS.[23] This difference is linearly proportional to the amplitude of ω. In the region from $t=-0.3$ to -0.7 $(\mathrm{GeV}/c)^2$, this difference is substantial and positive, so not both the ss amplitude and the sn amplitude of ω can vanish in this region. If the ω trajectory is not drastically different from the ρ trajectory, it has to pass through zero in this t interval, and we believe mechanism (1) is natural for the ω.

From the πN and NN analysis, we found that it is most natural for the P' trajectory to choose mechanism (4). This is discussed in Secs. III and IV. The P trajectory, because of its small slope, does not pass through zero in the t region we analyzed, and we cannot decide which mechanism is preferred. For uniformity, we choose mechanism (4) for the P trajectory.

III. PHENOMENOLOGICAL ANALYSIS OF THE $\pi^{\pm}p$ DATA

In this section we shall discuss our fits both with the no-compensation mechanism and with the Chew mechanism. Analogously to Ref. 8, with the no-compensation mechanism for P and P', we parametrize the ss and sn amplitudes, or the A' and B amplitudes for the pion-nucleon scattering, as follows:

$$\begin{aligned}
f_{ss}&\equiv\tfrac{1}{4}(4M_N{}^2-t)^{1/2}A',\\
&=(1-t/4M_N{}^2)^{-1/2}\alpha^2(\alpha+1)^2\xi C_0\exp(C_1t)(E_L/E_0)^{\alpha}\\
&\qquad\qquad\text{for } P \text{ and } P',\\
&=(1-t/4M_N{}^2)^{-1/2}(\alpha+1)\xi C_0[(1+C_2)\exp(C_1t)\\
&\qquad -C_2](E_L/E_0)^{\alpha}\quad\text{for } \rho,\\
f_{sn}&\equiv\tfrac{1}{8}[t(t-4M_\pi{}^2)]^{1/2}B\\
&=[-t(1-t/4M_\pi{}^2)]^{1/2}\alpha^2(\alpha+1)\xi D_0\\
&\qquad\times\exp(D_1t)(E_L/E_0)^{\alpha-1}\quad\text{for } P \text{ and } P',\\
&=[-t(1-t/4M_\pi{}^2)]^{1/2}\alpha(\alpha+1)\xi D_0\\
&\qquad\times\exp(D_1t)(E_L/E_0)^{\alpha-1}\quad\text{for } \rho,
\end{aligned}$$

[18] Y. Hara, Phys. Rev. **136**, B507 (1964); L. L. Wang, *ibid.* **142**, 1187 (1966). See also Ref. 14.

[19] G. Chew, Phys. Rev. Letters **16**, 60 (1966).

[20] M. Gell-Mann, in *Proceedings of the 1962 International Conference on High-Energy Nuclear Physics at CERN* edited by J. Prentke (CERN, Geneva, 1962), p. 539.

[21] We mention here the following possible backgrounds: (a) a resonance tail, (b) another low-lying trajectory, (c) a Mandelstam-Regge-cut contribution, and (d) a complex trajectory function with a small imaginary part.

[22] K. J. Foley, S. J. Lindenbaum, W. A. Love, S. Ozaki, J. J. Russell, and L. C. L. Yuan, Phys. Rev. Letters **11**, 425 (1963).

[23] (a) Differential-cross-section data: B. Cork and W. A. Wenzel, Phys. Rev. **107**, 859 (1957); A. R. Clyde, Ph.D. thesis, University of California, Berkeley 1966 (unpublished); O. Czyzewski, B. Escoubés, Y. Goldschmidt-Clermont, M. Guinea-Moorhead, D. R. O. Morrison, and S. de Unamuno-Escoubés, Phys. Letters **15**, 188 (1965); B. Escoubés, A. Fedrighini, Y. Goldschmidt-Clermont, M. Guinea-Moorhead, T. Hofmokl, R. Lewisch, D. R. O. Morrison, M. Schneeberger, S. de Unamuno, H. C. Dehne, E. Lohrmann, E. Raubold, P. Södig, M. W. Teucher, and G. Wolf, *ibid.* **5**, 132 (1963); K. J. Foley, R. S. Gilmore, S. J. Lindenbaum, W. A. Love, S. Ozaki, E. H. Willen, R. Yamada, and L. C. L. Yuan, Phys. Rev. Letters **15**, 45 (1965). (b) Polarization data: M. Borghini, G. Coignet, L. Dick, K. Kuroda, L. diLella, A. Michalowicz, P. C. Macq, and J. C. Olivier, in *Proceedings of the Thirteenth International Conference on High-Energy Physics, Berkeley, 1966* (University of California Press, Berkeley, 1967).

TABLE I. Regge parameters for pion-nucleon amplitudes (see Ref. 24).

	No-compensation mechanism for P and P'			Chew mechanism for P and P' Case (a)			Case (b)		
	P	P'	ρ	P	P'	ρ	P	P'	ρ
C_0 (mb GeV^2)	2.16	7.49	0.70	$2.07\times\alpha_0(\alpha_0+1)$	$7.00\times\alpha_0(\alpha_0+1)$	0.66	$2.22\times\alpha_0(\alpha_0+1)$	$7.75\times\alpha_0(\alpha_0+1)$	0.69
C_1 (GeV^{-2})	1.16	−1.92	2.00	1.10	2.66	2.66	1.26	1.59	0.19
C_2	...	...	1.98	...	...	1.66	...	...	18.9
D_0 (mb GeV)	...	...	1.03	1.19	0.83	1.02	−0.31	−0.26	0.94
D_1 (GeV^{-2})	...	...	0.053	5.20	−1.53	−0.087	5.39	−2.75	0.04
α_0	1.00	0.63	0.58	1.00	0.66	0.59	1.00	0.62	0.58
α_1 (GeV^{-2})	0.33	1.31	1.03	0.49	1.44	1.13	0.45	1.63	1.00
α_2 (GeV^{-4})	...	0.29	...	...	0.32	0.15	...	0.42	0.01

where

$$\xi\equiv-[\exp(-i\pi\alpha)\pm1]/\sin\pi\alpha,$$
$$\alpha(t)=\alpha(0)+\alpha_1(t) \quad \text{for } P \text{ and } \rho,$$
$$\alpha(t)=\alpha(0)+\alpha_1 t+\alpha_2 t^2 \quad \text{for } P', \qquad (3.1)$$

where E_L is the incident pion lab energy and E_0 is the scale factor conveniently chosen to be 1 GeV/c. Since in fitting the secondary bump, we assume the contribution of P' is dominating, and the form of the P' trajectory is more crucial than that for P and ρ, we approximate the P' trajectory by a second-order power series. With the Chew mechanism for P and P', in the ss amplitude one replaces the $\alpha^2(\alpha+1)^2$ factor by $\alpha(\alpha+1)$, and in the sn amplitude the parametrization is the same as above.

The 2- to 5-GeV/c elastic DCS data points as displayed in Fig. 1 together with some sample high-energy data points are included in the least-square analysis. The high-energy information used is essentially the same as that used in Ref. 8, which also has detailed references. This includes the total cross sections, differential cross sections for elastic scattering, the differential cross sections for charge-exchange scattering, the phase of the forward elastic scattering amplitude at various energies obtained by Coulomb interference measurements, the constraint on the zero intercept of P' obtained from the dispersion relation on the real part of the forward scattering amplitude at zero energy, and the constraints on the f_{ss} and f_{sn} amplitudes at the position of the physical ρ meson from the knowledge of nucleon electromagnetic structure. We also include more up-to-date $\pi^- p$ polarization data[23] than those used in Ref. 8. The recent CERN $\pi^+ p$ polarization results[23] are also incorporated.

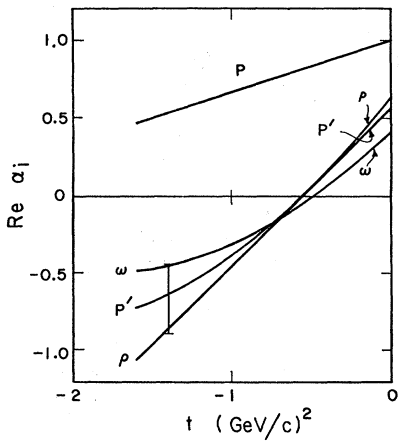

FIG. 2. The Regge trajectories P, P', ρ, and ω determined for no-compensation solution in $t<0$ region. The point I indicates the range of α_{eff} value determined from model-independent analysis at $t=-1.4$ (GeV/c)^2 [see Eq. (1.2)].

With the no-compensation mechanism, our fit to the high-energy data points is of comparable quality to that presented in Ref. 8. The parameters of this solution are tabulated in Table I.[24] The detailed χ^2 comparisons are listed in Table II. The quality of the fit to the secondary bump is illustrated in Fig. 1. In view of the fact that we have not incorporated explicitly the direct-channel resonance contribution and our simple parametrization is now applied over a large t region, we feel the essential feature of the dip-bump structure is reproduced reasonably well in our present fit. The tabulated trajectory functions are also illustrated in Fig. 2. The P' trajectory is quite well determined. In our fit, the dip in the $\pi^\pm p$ DCS is formed due to the vanishing of $\alpha_{P'}$ at $\alpha_{P'}=0$ with a smooth and rapidly falling $|f_{ss}{}^P|^2$ term. Since the $|f_{ss}{}^P|^2$ term is substantial, the position of the dip has shifted considerably from $\alpha_{P'}=0$. In our fit $\alpha_{P'}$ passes through zero near $t=-0.5$, whereas the dip is at -0.8. Unlike the dip in the charge exchange, the fit shown in Fig. 1 moves out slightly as the energy is increased, because the $|f_{ss}{}^P|^2$ term decreases more slowly than the $|f_{ss}{}^{P'}|^2$ term. The data do not indicate any dip in the region between $t=-1.0$ and -2.0. Since the contribution of $f_{ss}{}^{P'}$ is used to explain the secondary bump, from Eq. (3.1) one sees that $\alpha_{P'}$ cannot pass through -1 in this region. The P' trajectory shown in Fig. 2 is consistent with the

[24] Note the following: (a) The relation between C_0's defined for the no-compensation mechanism and those defined by the Chew mechanism is

$$\alpha_0^2(\alpha_0+1)^2 C_0{}^{\text{nc}}=\alpha_0(\alpha_0+1)C_0{}^{\text{Ch}}.$$

(b) The C_0's and D_0's defined for the Chew mechanism here are related to the C_0's and D_0's of Ref. 8 by

$$C_0{}^{\text{Ch}}=\tfrac{1}{2}MC_0, \quad D_0{}^{\text{Ch}}=\tfrac{1}{4}M_\pi D_0.$$

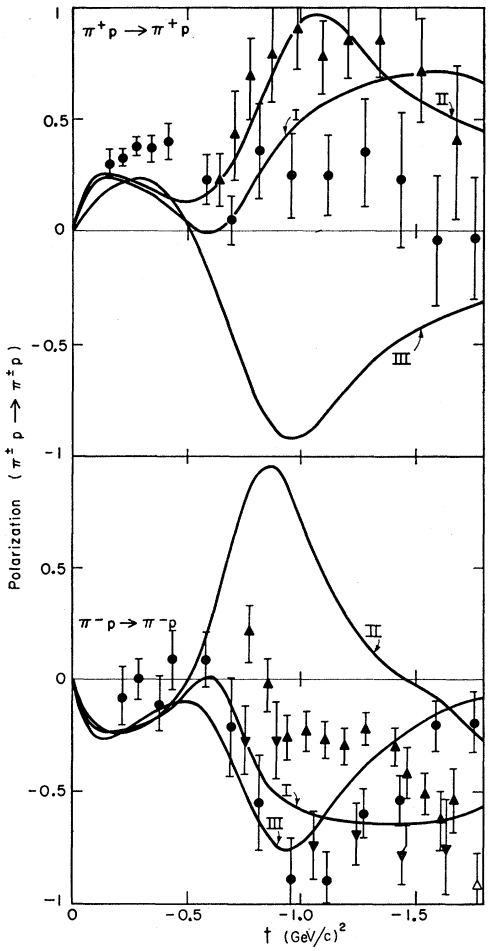

FIG. 3. $\pi^\pm p$ polarization data compared with our Regge predictions. π^+p—▲ 1.988 GeV/c, ● 2.535 GeV/c; π^-p—▲ 1.988 GeV/c, ● 2.535 GeV/c, ▼ 2.912 GeV/c. All data points are taken from Ref. 26. Curves I are predicted by no-compensation solution, curves II and III are predicted by the Chew mechanism, case a and case b, respectively, at 2.5 GeV/c.

model-independent analysis at $t=-1.4$ (GeV/c)^2, and does not pass through -1. The ρ trajectory we used here is essentially the same as that of Ref. 8. As shown by various authors,[5] it is in reasonable agreement with the values obtained through model-independent analysis. The zero intercept of P is assumed to be unity. The slope of P is found unlikely to be above 0.4 (GeV/c)$^{-2}$. In our fit,[25] for the no-compensation mechanism its value is between 0.3 and 0.4. The data, with good statistics, indicate no noticeable structure in the $\pi^\pm p$ forward diffraction peak. This constrains the two amplitudes $f_{sn}{}^P$ and $f_{sn}{}^{P'}$ to be small in the small $|t|$ region. Their values in the large $|t|$ region are poorly known. We fitted the data both with and without $f_{sn}{}^P$ and $f_{sn}{}^{P'}$ amplitudes. We found the χ^2 for these two cases are essentially the same. The solution presented in this paper has both $f_{sn}{}^P$ and $f_{sn}{}^{P'}$ set to zero.

TABLE II. Data fitted (χ^2).

Type	Number of data points	No-compensation	Chew mechanism Case (a)	Chew mechanism Case (b)	Ref. 8 Case (a)	Ref. 8 Case (b)
$(d\sigma/dt)(\pi^\pm p)$	141	154	371	258	133	161
$\sigma_T(\pi^\pm p)$	16	8	9	8	10	7
$P(\pi^\pm p)$	85	155	314	203	...[a]	...
$(d\sigma/dt)(\pi^- p \to \pi^0 n)$	56	88	87	88	87	87

[a] The $\pi^\pm p$ polarization data fitted in the present paper were not available then. We found, with the inclusion of these polarization data in the fit, the best χ^2 value would be $\approx$130 for the analysis of Ref. 8.

With P and P' parametrized according to the Chew mechanism, our fits are less satisfactory. We searched for the following two different possibilities. For case (a), the signs for the coefficients D_0 in both $f_{sn}{}^P$ and $f_{sn}{}^{P'}$ are chosen to be negative, which is consistent with the solutions in Ref. 8. The best χ^2 obtained in this case is about a factor of two larger than the no-compensation solution. For case (b), both of these signs are chosen to be positive. This notably improves the situation. But the χ^2 obtained is still not quite comparable to that with the no-compensation mechanism. The parameters and the detailed χ^2 for both cases are also given in Tables I and II.

With the no-compensation mechanism, the $\pi^\pm p$ polarization in the secondary bump region is contributed mainly by the interference between $f_{ss}{}^{P'}$ and $f_{sn}{}^{\rho}$. Figure 3 shows a typical prediction on π^+p and π^-p polarization (curves I) together with some sample data points.[26] Generally speaking, near the position of the

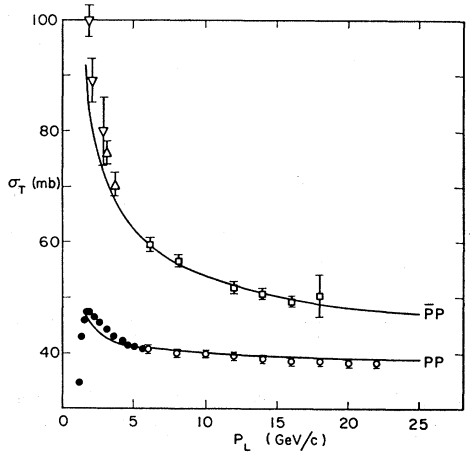

FIG. 4. pp and $\bar{p}p$ total-cross-section data compared with our fit of non-compensation solution. Data points □, ○ Galbraith *et al.*, ▽ Armenteros *et al.* (Ref. 28), and △ Escoubés *et al.* (Ref. 23), ● Bugg *et al.* (Ref. 28).

[25] Due to the zero in the $f_{ss}{}^{P'}$, the contribution of P' to the *dcs* is steeper than that of P. In addition, the contribution of P' falls off faster than that of P as energy increases. With these two factors, the P' contribution gives an antishrinkage effect.

[26] O. Chamberlain, M. J. Hansroul, C. H. Johnson, P. D. Grannis, L. E. Holloway, L. Valentin, P. R. Robrish, and H. M. Steiner, Phys. Rev. Letters **17**, 975 (1966).

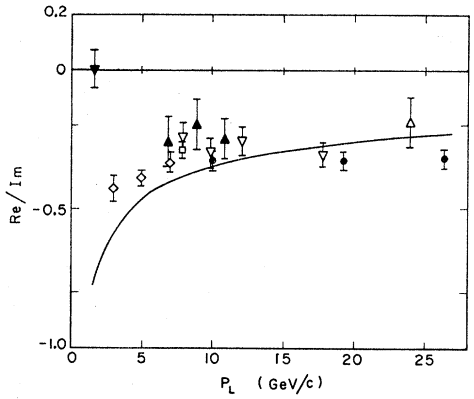

FIG. 5. The data on the ratio Re/Im of the forward scattering amplitude for pp scattering compared with our Regge prediction. Data points: △ Lohrman *et al.*, ○ Bellitini *et al.*, ▽ Foley *et al.*, □ Taylor *et al.*, ▲ Kirillora *et al.*, ◇ Clyde *et al.*, and ▼ Dowell *et al.* (see Ref. 29).

secondary bump the predicted polarization for π^+p and for π^-p by this solution should have opposite sign, because the ρ contributes oppositely. In our solution for the Chew mechanism, the polarization is contributed mainly by the interference between $f_{ss}{}^P$ and $f_{sn}{}^{P'}$. It predicts a large polarization with the same sign for π^+p and π^-p (see Fig. 3, curves II and III). The existing $\pi^\pm p$ polarization data in this energy- and momentum-transfer region indicate the gross trend of having opposite sign. This we interpret to mean that the data are in favor of the no-compensation type of solution. We note here that the data also show significant variation from energy to energy. This implies that even though the resonance amplitudes do not play an important role in the DCS, they could play a substantial role in the polarization. This is because the polarization depends more critically on the relative phases between various amplitudes. To fit the experimental data quantitatively, one has to take into account the resonance contribution explicitly.[27]

To summarize, we have shown here that if one assumes the Regge amplitude can be simply extrapolated to the lower energy and larger $|t|$ region, neglecting the resonance contribution the data prefer the no-compensation mechanism over the Chew mechanism for the P' trajectory.

IV. PHENOMENOLOGICAL ANALYSIS OF THE pp AND $\bar{p}p$ DATA

The situation in the NN scattering is more complicated. The total-cross-section data[28] are shown in Fig. 4. The $\bar{p}p$ total cross section behaves smoothly in the high-energy region and starts to rise rapidly around 2.0 GeV/c. The pp total cross section behaves smoothly beyond 3 GeV/c, but at around 2 GeV/c starts to turn over. Since the Regge model gives only smooth behavior in the total cross section, this indicates, as expected, that the lower the energy is, the further the amplitudes deviate from pure Regge amplitudes. The existing Re/Im data[29] give further indication that the phase of the forward scattering amplitudes deviate from the pure Regge amplitudes in the low-energy region. The data for this ratio are shown in Fig. 5. For the 6- to 20-GeV/c region, although varying significantly from experiment to experiment, it ranges from -35% to -20%. Although the measurement by Clyde *et al.*[23] gives $-43\pm5\%$ at 3 GeV/c, around 1.8 GeV/c this ratio vanishes and becomes positive at lower energy.[29] So the turning point could be around 2.5 GeV/c. The ratio predicted by the Regge-pole model increases in magnitude monotonically as the energy decreases. As is discussed below, the highest energy at which the dip-bump structure in the $\bar{p}p$ DCS is clearly observed[30,31] is at 2.5 GeV/c and $0.4<|t|<1.0$. We would like to push the Regge-pole model to as low as 2.5 GeV/c. From the above discussion we do not expect a quantitative agreement with experiment in this region. However, the πN analysis described in the previous section does give support to the assumption that although the phase of the amplitude given by the Regge-pole model deviates from the observed value at low energy, the magnitude of the amplitude given by the Regge-pole model is still dominating and can be used to explain the gross feature of the experimental data in the region of interest.[32]

A sample of pp and $\bar{p}p$ elastic DCS data is shown in Fig. 6. The pp data at 3, 5, and 7 GeV/c were recently measured by Clyde *et al.*, and those at 19.6 GeV/c by Foley *et al.*[23] These data indicate that the pp forward peak are less steep than the $\bar{p}p$ peak, and it exhibits shrinkage as the energy increases. The pp DCS do not exhibit any structure. The $\bar{p}p$ DCS at 2 and 2.5 GeV/c were measured by Barish *et al.*[30,31] of the California

[27] We thank Dr. A. V. Stirling of Saclay for discussions on this point when he was visiting at the Lawrence Radiation Laboratory, 1966.

[28] W. Galbraith, E. W. Jenkins, T. F. Kycia, B. A. Leontic, R. H. Phillips, and A. L. Read, Phys. Rev. **138**, B913 (1965); D. V. Bugg, D. C. Salter, and G. H. Stafford, *ibid.* **146**, 980 (1966); R. Armenteros, C. A. Coombes, B. Cook, G. R. Lambertson, and W. A. Wenzel, *ibid.* **119**, 2068 (1960).

[29] J. D. Dowell, R. J. Homer, Q. H. Khan, W. K. McFarlane, J. S. C. Mckee, and A. W. O'Dell, Phys. Letters **12**, 252 (1964); H. Lohrmann, H. Meyer, and H. Winzeler, *ibid.* **13**, 78 (1964); A. E. Taylor, A. Ashmore, W. S. Chapman, D. F. Falla, W. H. Range, D. B. Scott, A. Astbury, F. Capocci, and T. G. Walker, *ibid.* **14**, 54 (1965); K. J. Foley, R. S. Gilmore, R. S. Jones, S. J. Lindenbaum, W. A. Love, S. Ozaki, E. H. Willen, R. Yamada, and L. C. L. Yuan, Phys. Rev. Letters **14**, 74 (1965); G. Bellettini, G. Cocconi, A. N. Diddens, E. Lillethun, J. Pahl, J. P. Scanlon, J. Walters, A. M. Wetherell, and P. Zanella, Phys. Letters **14**, 164 (1965). See also Clyde *et al.* (Ref. 22).

[30] B. Barish, D. Fong, R. Gomez, D. Hartill, J. Pine, A. V. Tollestrup, A. Maschke, and T. F. Zipf, California Institute of Technology Report, 1966 (unpublished).

[31] B. Barish, D. Fong, R. Gomez, D. Hartill, J. Pine, A. V. Tollestrup, A. Maschke, and T. F. Zipf, Phys. Rev. Letters **17**, 720 (1966).

[32] A similar assumption was first made by Frautschi (Ref. 10), in which he discussed the possibility of explaining the feature of $\bar{p}p$ dip-bump structure in the energy region from 1.6 to 2.5 GeV/c by using the Regge-pole model.

Institute of Technology group, at 3 and 4 GeV/c, respectively, by Escoubés *et al.* and by Czyzewski *et al.* at CERN,[23] and at 12 GeV/c by Foley *et al.* at Brookhaven.[23]

The $\bar{p}p$ DCS shown in Fig. 6 have appreciable structure beyond $t=-0.4$ (GeV/c)^2. The one at 2.5 GeV/c has a pronounced dip near $t=-0.5$, followed by a secondary bump. The energy dependence of the magnitude of the bump is not absolutely clear at present. The Caltech data between 1.5 and 2.5 GeV/c indicate a monotonic fall of the magnitude of the bump. This trend is continued in the 3-GeV/c CERN data, but it is puzzling that the magnitude of the bump between the t interval from -0.6 to -1.0 (GeV/c)^2 at 4 GeV/c should be so similar to that at 3 GeV/c. There is also the complication that the Caltech data have a 50% normalization uncertainty.[33] Unfortunately, no $\bar{p}p$ data are available above 4 GeV/c in the same t region to give a definite statement about this energy dependence. However, combining all the available experimental information, as is suggested in Refs. 31 and 10, we consider it plausible that the magnitude of the secondary maximum should decrease with the increase of energy. The dissimilarity between pp and $\bar{p}p$ DCS for $|t|<1$ can be summarized as follows: The pp forward peak is relatively flat, it is smooth and without noticeable structure, and the peak shrinks with the increase of energy; whereas the $\bar{p}p$ forward peak is relatively steep, the $\bar{p}p$ DCS show appreciable structure in the lower s and larger $|t|$ region, and the forward peak "antishrinks."

Now let us discuss in some detail the actual analysis and the assumptions involved here. For the pp and $\bar{p}p$ elastic scattering P, P', ω, ϕ, ρ, π, and all other known nonstrange meson trajectories can be exchanged. From the study of the total-cross-section data of pp and $\bar{p}p$ and the comparison[34] between the total cross section of pp, pn, $\bar{p}p$, and $\bar{p}n$, one finds that the contribution of P, P', and ω to the ss amplitudes should be dominating. There is less information on the magnitude of sn and nn amplitudes. As mentioned in Sec. III, the sn amplitudes in the πN analysis for both P and P' in the small $|t|$ region are small, in fact they can be set to zero. From factorization we expect the sn and nn amplitudes should also be small compared with the ss amplitudes. In NN scattering, near the forward direction, the pp and $\bar{p}p$ elastic DCS do not have any noticeable structure. This implies that the contributions of sn and nn amplitudes of P, P', ω, and all the other trajectories cannot be important here. On the other hand, about 10 to 20% polarization has been observed[35] in the t region from -0.1 to -0.7. This implies that the sn amplitudes and in turn the nn amplitudes certainly are present. However, we found that in explaining the $\bar{p}p$ dip-bump structure together with the pp smooth behavior in the 2.5- to 4-GeV/c region it is not crucial whether one includes the nonsense amplitudes or not, although the behavior of $\bar{p}p$ DCS at higher energy and large $|t|$ region does depend quite sensitively on the magnitude of the nonsense amplitudes. Presently no experimental DCS at higher energies are available. Since we only try to get a reasonable fit to the existing DCS data, for simplicity we neglect all the sn and nn amplitudes. Thus we write

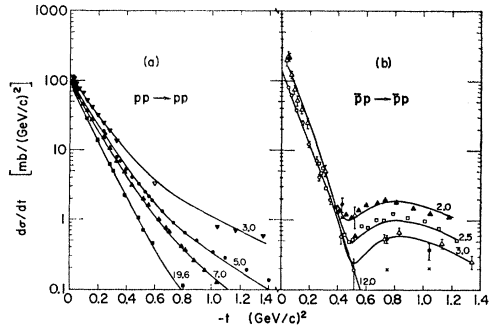

FIG. 6. The pp and $\bar{p}p$ differential cross sections. The pp data: at 3, 5, and 7 GeV/c are from Clyde *et al.* in Ref. 23, at 19.6 GeV/c from Foley *et al.* in Ref. 3. The $\bar{p}p$ data: at 2.0 and 2.5 GeV/c from Barish *et al.* in Refs. 30 and 31 at 3.0 GeV/c from Escoubés *et al.* in Ref. 23, at 4 GeV/c from Czyzewski *et al.* in Ref. 23, and at 12 GeV/c from Foley *et al.* in Ref. 23. Values of the fitted DCS by integrating over corresponding bin intervals: × inside △ 3 GeV/c, ×4 GeV/c.

$$\frac{d\sigma}{dt}=\frac{1}{4\pi s p^2}|f_{ss}{}^P+f_{ss}{}^{P'}\pm f_{ss}{}^{\omega}|^2, \tag{4.1}$$

where the + sign is for $\bar{p}p$ and the − sign is for pp, and

$$f_{ss}{}^i=(1-t/4M^2)^{-1}\alpha_i{}^2(\alpha_i+1)^2\xi_i C_{ss}{}^i \times\exp(D_{ss}{}^i t)(E/E_0)^{\alpha_i}, \tag{4.2}$$

with i being P or P',

$$f_{ss}{}^{\omega}=(1-t/4M^2)^{-1}(1-t/t_0)(\alpha_\omega+1)\xi_\omega C_{ss}{}^{\omega} \times\exp(D_{ss}{}^{\omega}t)(E/E_0)^{\alpha_\omega}, \tag{4.3}$$

and

$$\xi\equiv-[\exp(-i\pi\alpha)\pm1]/\sin\pi\alpha.$$

The extra factor $(1-t/t_0)$ in the $f_{ss}{}^{\omega}$ amplitude is necessary in order to explain the change in sign of the

[33] The $\bar{p}p$ differential cross section by the Cal Tech group is a sum of forward and backward scattering. The contribution of the backward scattering has been estimated by taking the average of the backward $\bar{p}p$ data at 1.6 and 4 GeV/c (see Lynch *et al.*, below, and Czyzewski *et al.*, Ref. 23, respectively), and subtracted from the original data. We also like to point out that the values of the $d\sigma/dt$ should be half of the published values shown in Fig. 1 of Ref. 35. But the values of $d\sigma/dt$ of Table I in Ref. 34 are correct, as confirmed by Dr. A. V. Tollestrup. For $\bar{p}p$ data at 1.6 GeV/c, see G. R. Lynch, R. E. Foulks, G. R. Kalbfleisch, Sylvia Limentani, J. B. Shafer, M. L. Stevenson, and N. Xuong, Phys. Rev. **131**, 1276 (1963).

[34] For instance, see W. Rarita and V. L. Teplitz, Phys. Rev. Letters **12**, 206 (1964); T. O. Binford and B. R. Desai, Phys. Rev. **138**, B1167 (1965).

[35] P. Grannis, J. Arens, F. Betz. O. Chamberlain, B. Dieterle, C. Schultz, G. Shapiro, H. Steiner, L. Van Rossum, and D. Weldon, Phys. Rev. **148**, 1297 (1966).

TABLE III. Regge parameters for nucleon-nucleon amplitudes.

	P	P'	ω
C_0 (mb GeV^2)	7.84	27.9	17.4
C_1 (GeV^{-2})	2.41	−1.39	1.50
t_0 (GeV^2)	···	···	−0.15
α_ω		$0.41+0.99t+0.27t^2$	

difference $(d\sigma_{pp}/dt)-(d\sigma_{\bar{p}p}/dt)$, and t_0 is the position of the crossover point. The trajectories α_P and $\alpha_{P'}$, have already been determined in the πN analysis. We parametrize $\alpha_\omega=\alpha_\omega{}^0+\alpha_\omega{}^1t+\alpha_\omega{}^2t^2$.

We include the pp and $\bar{p}p$ DCS data shown in Fig. 6 together with the pp and $\bar{p}p$ total-cross-section data shown in Fig. 4 for $p_L>2.5$ GeV/c in making a least-squares fit. The coefficients $C_{ss}{}^P$, $C_{ss}{}^{P'}$, $C_{ss}{}^\omega$, and $\alpha_\omega{}^0$ are essentially determined from the information on $\sigma_T{}^{pp}$, $\sigma_T{}^{\bar{p}p}$, and $d\sigma/dt(t=0)|_{pp,\bar{p}p}$. The best-fit values for these parameters are shown in Table III. The fits to the total-cross-section data are shown in Fig. 4. It fits the high-energy data quite well. At 2.5 GeV/c our fits for both pp and $\bar{p}p$ data are slightly less than 10% lower than the experimental data points. The Re/Im ratio for our solution is shown in Fig. 5. Between 10 and 20 GeV/c it varies from 35 to 26%, consistent with the data, although the rate of decrease seems to be a little bit too fast. This ratio deviates from the data significantly in the low-energy region, as expected, but it gives the correct sign and magnitude down to 2.5 GeV/c. We believe the gross feature of the DCS can still be explained by the Regge-pole model.

The three exponents $D_{ss}{}^P$, $D_{ss}{}^{P'}$, and $D_{ss}{}^\omega$, together with $\alpha_\omega{}^1$ and $\alpha_\omega{}^2$, are the adjustable parameters used to fit the t dependence of $(d\sigma/dt)_{pp}$ and $(d\sigma/dt)_{\bar{p}p}$. Our fitted curves to pp and $\bar{p}p$ data are illustrated in Fig. 6. The parameters for the best-fit solution are also given in Table III. In our solution, $f_{ss}{}^{P'}$ is small around the dip region because of its zero at $\alpha_{P'}=0$. The dip-bump structure is mainly produced by the interference between $f_{ss}{}^P$ and $f_{ss}{}^{P'}$. In the pp case, $f_{ss}{}^P$ interferes with $f_{ss}{}^\omega$ with opposite sign and gives a smooth and dominating contribution. The zero in $f_{ss}{}^{P'}$ at $\alpha_{P'}=0$ gives the slight curvature in the pp DCS in the large $|t|$ region. Although the $\bar{p}p$ DCS data at 2.0 GeV/c were not included in the search, we found, as illustrated, that our solution also gives a prediction at this energy that is reasonable compared with the data.

In Fig. 6 the $\bar{p}p$ datum point at 3 GeV/c near $t=-0.5$ is much higher than the actual curve. But the integrated area obtained from our fitted curve for the corresponding bin interval of the relevant datum point gives the value indicated in the figure. One sees that it is within one standard deviation of the allowed value. Our fit to the two points at larger $|t|$ values is also reasonable. An estimate is also made to obtain the area for the bin interval represented by the point near $t=-0.4$ for 4 GeV/c, and again the agreement is similar to that for the corresponding point at 3 GeV/c. Our prediction for the larger $|t|$ points at 4 GeV/c as shown is about a factor of 2 lower than the experimental data. This reflects the puzzling fact, as mentioned earlier, that the magnitude of the secondary bump at 4 GeV/c should be so similar to that at 3 GeV/c. To really clarify the situation we suggest that an accurate measurement of pp elastic DCS at 3 GeV/c from $t=-0.3$ to $t=-1.0$ be made, to complement the data by Clyde *et al.*, although it is very plausible that the behavior will be smooth from the 5- and 7-GeV/c measurements in the same t region. Probably more important are accurate measurements of the $\bar{p}p$ DCS in the t region from -0.4 to -1.0 (GeV/c)^2 and energy range from 2.0 to 8.0 GeV/c. Then we can really pin down the energy dependence of the magnitude of the secondary bump. Furthermore, if measurements of $\bar{p}p$ polarization in the similar region become available we can then, by analyzing them together with presently available $\bar{p}p$ polarization data,[35] put in all the nonsense amplitudes, consistent with πN fit through factorization, and make a more accurate test of the validity of our results.

ACKNOWLEDGMENTS

We thank Professor Geoffrey F. Chew for suggesting this study and for his advice throughout the development of this work. We are grateful to Professor Stanley Mandelstam for his interest in this work and invaluable discussions. We are indebted to Dr. Roger J. N. Phillips and Dr. Vernon Barger for their contribution in the πN analysis using the Chew mechanism prior to the development of this work. We also thank Dr. A. V. Stirling for helpful discussions.